Time Evolution of Structures under Shear-Induced Phase Separation and Crystallization in Semidilute Solution of Ultrahigh Molecular Weight Polyethylene†

Hiroki Murase,‡ Takuji Kume,§ and Takeji Hashimoto*

Department of Polymer Chemistry, Graduate School of Engineering, Kyoto University, Katsura, Nishikyo-ku, Kyoto 615-8510, Japan

Yasuo Ohta

Corporate Research Center, TOYOBO Co., Ltd., 2-1-1, Katata, Ohtu-shi, Shiga 520-0292, Japan

Received January 15, 2005; Revised Manuscript Received July 29, 2005

ABSTRACT: We investigated shear-induced structures for a semidilute solution of ultrahigh molecular weight polyethylene (UHMWPE) with a paraffin wax as a solvent by means of shear small-angle light scattering, shear microscopy, birefringence, and rheology. The solution has a reduced concentration (c/c^* where c and c^* is concentration and the overlap concentration, respectively) of 11 and hence well-developed entanglements. The structures were investigated at temperature of 124 °C, which is approximately equal to the equilibrium melting temperature of crystals in the solution at quiescent state. We found both shear-induced liquid−liquid phase separation and shear-induced crystallization, when the solution was subjected to shear flow at shear rate larger than the critical shear rate $\dot{\gamma}_{c,streak}$. Time change in the shear-induced structures after onset of the shear at $\dot{\gamma} > \dot{\gamma}_{c,streak}$ or after cessation of the same shear illuminated that the shear-induced phase separation triggers the shear-induced crystallization into fibrous structures: crystallization occurs through regions rich in polymer concentration that are built up by the shear.

I. Introduction

When semidilute polymer solutions are subjected to shear flow with shear rate $\dot{\gamma}$ greater than a critical value, the solutions become turbid because of the liquid−liquid phase separation or the enhancement of concentration fluctuations induced by the shear.[1−3] This intriguing phenomenon is explained theoretically as a consequence of dynamical coupling between stress and diffusion[4−8] inherent in dynamically asymmetric systems in which constituent elements have a considerable dispersity in mobilities. In our previous papers,[9,10] we reported that the shear-induced phase separation was observed also in semidilute, athermal solutions of ultrahigh molecular weight polyethylene (UHMWPE) solutions with a paraffin as a solvent. Moreover, development of shear-induced crystallization was observed in addition to the shear-induced phase separation when the solutions were sheared at a temperature 124 °C, close to the equilibrium melting temperature of crystals in the quiescent solution.[10]

It is well-known that the fibrous crystalline superstructure having a characteristic morphology of so-called "shish kebab" was grown in stirred dilute or semidilute solutions of polyethylene.[11,12] Many efforts have been made to elucidate the mechanism of formation of the shish-kebab structure, but it is still not completely clarified. It should be emphasized that there are few researches concerning relationships between the shear-induced phase separation and the shear-induced crystallization, except for the extensive works reported by McHugh and co-workers.[13−17]

McHugh and co-workers reported a series of interesting and important rheooptical works of polyethylene and polypropylene solutions in tubular shear flow geometry.[13−15] Their studies elucidated phenomena of liquid−liquid "precursor formation" (phase separation) and subsequent fibrillar shish-kebab crystallization. Although our work is directed along the same line as these preceding works, there is an important difference between our works and these previous works. Our work is concerned with well-entangled semidilute athermal solutions of UHMWPE, while their works are concerned with dilute solutions in xylene with no entanglements.

Although both systems have common characteristics resulting from the constituents in the system having dynamical asymmetry, the way how the elastic effects influence shear-induced phase separation and shear-induced crystallization should be quite different. In a more general term, nonequilibrium pathways, by which dissipative structures (ordered structures developed in open nonequilibrium systems) are formed, are expected to be very different. This may become obvious if one considers differences between the two systems in terms of the stress level involved and in the level of the concentration fluctuations built up prior to crystallization. At this stage we do not know how we can interrelate the behaviors of the two different systems. Therefore, we shall treat the problems involved by our semidilute solutions separately from those involved by their dilute solutions, although their works are still very informative. Moreover, as for semidilute crystallizable solutions having well-developed entanglements, there

† Presented in part at 43th Polymer Symposium, Soc. Polym. Sci., Jpn., Polym. Prepr. Vol. 43, p 3490 (1994), 45th Polymer Symposium, Soc. Polym. Sci., Jpn., Polym. Prepr. Vol. 45, p 3380 (1996), and International Symposium on Fiber Science and Technology (1994, Yokohama, Japan).

‡ Present address: Corporate Research Center, TOYOBO Co., Ltd., 2-1-1, Katata, Ohtu-shi, Shiga 520-0292, Japan.

§ Present address: Kao Corporation, Skin Care Research Labs., 2-1-3, Bunka Sumida-ku, Tokyo 131-8501, Japan.

* To whom correspondence should be addressed. E-mail: hashimoto@alloy.polym.kyoto-u.ac.jp.

10.1021/ma050092i CCC: $30.25
Published on Web 09/21/2005

have been still no works reported concerning relationship between shear-induced phase separation and crystallization into optically anisotropic fibrillar structures. It is our primary objective in this work to elucidate this relationship for the semidilute solutions.

We have performed shear-SALS (small-angle light scattering) experiments for the semidilute solution of UHMWPE to explore shear-induced structures as a function of $\dot{\gamma}$ at steady state.[10] Let us first summarize the previous results at 124 °C. From the scattering behavior as a function of $\dot{\gamma}$, the system could be classified into three shear regimes: At the regime where $\dot{\gamma}$ is lower than critical shear rate $\dot{\gamma}_{c,butterfly}$ for evolution of the butterfly pattern, the scattered intensity under the shear flow kept the same value as that of quiescent state (regime I). In the shear regime (regime II), where $\dot{\gamma}_{c,butterfly} < \dot{\gamma} < \dot{\gamma}_{c,streak}$, the critical shear rate for evolution of streak pattern, the butterfly pattern was developed, and the system could achieve a steady state under the shear flow. The facts that the sheared solution was optically isotropic and that the butterfly pattern disappeared after cessation of the shear suggest that the pattern arises from shear-enhanced concentration fluctuations or shear-induced liquid−liquid phase separation. In regime III where $\dot{\gamma} > \dot{\gamma}_{c,streak}$, the optically anisotropic streaklike pattern was developed perpendicular to the shear flow in addition to the butterfly pattern. The cross-polarized light scattering and the shear microscopy revealed developments of the streaklike pattern perpendicular to flow and optically anisotropic fibrils aligning along flow.

In this report, we focused on the time evolution of the shear-induced structures after onset of step-up shear flow from zero shear rate. After imposing given shear rates in the various shear regimes as described above on the solution at 124 °C, evolution of transient structures was observed by shear SALS, shear microscopy, birefringence, and rheology. In this work we would like to report that, at $\dot{\gamma} > \dot{\gamma}_{c,streak}$, crystallization occurred after the shear-induced phase separation, giving rise to optically anisotropic fibrous structures aligned parallel to flow. Further detailed studies of the shear-induced crystallization with these real-time and in-situ experiments will give useful information for getting insight into the relationship between the two phase transitions.

Before closing this section, let us briefly remark the large polydispersity of molecular weight in our sample. We believe that studies of effects of molecular weight distribution (MWD) on the shear-induced structures are extremely important. Thus, the studies with a very broad MWD are as important as those with a narrow MWD. In this series of studies we have been choosing a very broad MWD, simply because it is readily available and commercially important.

II. Experimental Methods

II-1. Sample. A commercial grade UHMWPE (Hizex240M, Mitsui Chemicals, Tokyo, Japan) was used for this experiment as a solute. The polymer has a weight-average molecular weight of $M_w = 2.0 \times 10^6$ and heterogeneity index $M_w/M_n = 12$, where M_n denotes the number-average molecular weight. Paraffin wax (Luvax1266: Nippon Seiro Co. Ltd., Tokyo, Japan) was used as a solvent. The molecular weight of the paraffin wax is ∼500 (producer's specification; measured by gas chromatography), and its melting point is 69 °C. The UHMWPE was dissolved in the paraffin wax with an antioxidant agent (2,6-di-*tert*-butyl-*p*-cresol), with 1 wt % of the total solution, using a screw-type extruder at 210 °C. Small particles

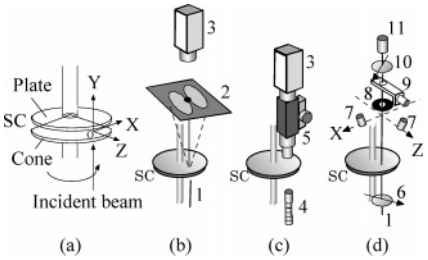

Figure 1. Schematic diagrams of (a) shear cell (SC) and coordinate system, (b) small-angle light scattering, (c) shear microscopy, and (d) shear birefringence: (1) incident He−Ne laser beam, (2) translucent screen, (3) CCD camera, (4) optical light guide for white halogen lamp, (5) microscope, (6) polarizer, (7) photodiodes for simultaneous measurement of light scattered intensity at two particular scattering vectors, (8) pinhole, (9) Berek compensator, (10) analyzer, (11) a photodiode for measurement of transmitted light intensity.

contaminating the solutions were filtered off by a mesh filter (400 lines/in.). This filtration process was highlighted to be very important for obtaining reliable data on the shear-induced structures and scattering in our previous works.[9,10] A 5 wt % solution having c/c^* of ∼11 was prepared (c^* is overlap concentration estimated from M_w). The equilibrium melting temperature T_d^0 of the crystals in the quiescent solution was estimated to be 123.9 ± 0.9 °C on the basis of the Hoffmann−Weeks plot,[18] as detailed elsewhere.[10] The highest nominal melting temperature for the quiescent solution was 118 °C.[10]

II-2. Shear SALS. The shear SALS experiments were carried out using a laboratory-made apparatus[19] in Kyoto University to record the scattering patterns with a CCD camera and a Macintosh computer system. The optical setup of the apparatus was identical to those described in the previous report.[10] A cone−plate type shear cell made out of quartz having the cone angle of 1° was used. The conventional coordinate system was applied as depicted in Figure 1a.

The optically transparent shear cell was filled with the sample, subsequently heated to 150 °C, and kept at 150 °C for more than 1 h to allow relaxation of the deformation and orientation of the UHMWPE induced during the charging of the sample in the shear cell. The solution was then cooled to an experimental temperature of 124 °C, approximately equal to $T_d^0 = 123.9 \pm 0.9$ °C. Steady shear flow with $\dot{\gamma}$ from 0.029 to 2.9 s^{-1} was imposed on the solution, and light scattering data were collected after the onset of the shear flow as a function of time t.

The scattered intensity distribution on the Oxz plane was qualitatively recorded by using a CCD video camera (Sony SSC-M370, Tokyo, Japan, part 3 in Figure 1b) and also on videotape by SVHS VCR(Victor HR-S6600,Yokohama, Japan) as analog movies and digitized with frame grabber board (RasterOps 24STV, Santa Clara, CA) mounted on the Macintosh computer. Here we report the scattering observed with a linearly polarized incident beam with polarization direction parallel to the Oz axis, unless otherwise stated, and with or without analyzer placed between the shear cell (SC) and the translucent screen (part 2 in Figure 1b) placed before the detector (part 3 in Figure 1b). The integrated scattered intensities as a function of time after the onset of shear flow, $\mathcal{I}_{\parallel}(t)$ and $\mathcal{I}_{\perp}(t)$ parallel to the x and z axis, respectively, defined below, were measured with the CCD camera.

$$\mathcal{I}_{\parallel}(t) = \int_{a_1}^{a_2} dq_x \int_{-\delta}^{\delta} dq_z \, I(q_x,q_z;t) \tag{1}$$

$$\mathcal{I}_{\perp}(t) = \int_{a_1}^{a_2} dq_z \int_{-\delta}^{\delta} dq_x \, I(q_x,q_z;t) \tag{2}$$

where $I(q_x,q_z;t)$ is the scattered intensity at time t where q_x and q_z are the x and z components of the scattering vector **q** whose magnitude q is defined by

$$q = (4\pi/\lambda)\sin(\theta/2) \tag{3}$$

with θ and λ being scattering angle and wavelength of light in the sample. In eqs 1 and 2, a_1, a_2, and δ were set at 1.77×10^{-4} nm^{-1}, 1.80×10^{-3} nm^{-1}, and 1.10×10^{-4} nm^{-1}, respectively.

II-3. Shear Microscopy. A white halogen lamp was used as a light source for the shear microscopy. The optical axis of the microscope was aligned parallel to the O*y* axis with an optical light guide (part 4 in Figure 1c), and therefore the structure development was observed under the same geometric arrangement as in the case of the shear SALS experiments. The fast shutter (as fast as 1/10000 s) and CCD video camera (part 3 in Figure 1b,c, Sony SSC-M370) was connected to the optical microscope (part 5 in Figure 1c). The images were recorded on videotape by the SVHS VCR as an analog movie and digitized with the frame grabber board mounted on the Macintosh computer in the similar way as shear SALS. The micrographs were saved digitally by image processing system. Thus, fast Fourier transform (FFT) was carried out from the images.[20] The FFT images were used to confirm whether microscope images truly represent the structural entity developed in the sheared solution by comparing the FFT spectrum with the corresponding light scattering patterns.

II-4. Shear Birefringence and Rheometry. A simultaneous measurement of shear birefringence and shear light scattering intensity at particular q's (defined by q_1's) was also performed. Optical setup of the measurement was schematically depicted in Figure 1d. A He−Ne laser light beam was sent along the O*y* axis (part 1), and transmitted light intensity under cross-polarization was measured by a photodiode (part 11). The polarization direction of the polarizer (part 6) was set at 90° with respect to that of the analyzer (part 10) and at 45° with respect to flow direction, as shown in Figure 1d. A retardation Γ_0 was initially added to the sample by the Berek compensator (part 9), and the retardation developed by shear flow Γ_s was calculated by the following equation:

$$I/I_0 = K\sin^2\{\pi(\Gamma_0 + \Gamma_s)/\lambda\} \tag{4}$$

where I, I_0, and K are transmitted light intensity of sample measured by a photodiode, incident beam intensity and a constant depending on the optical setup, respectively. Birefringence of the sheared solution was calculated by

$$\Delta n_{x-z} = (n_x - n_z) = \Gamma_s/d \tag{5}$$

where n_x, n_z, and d are refractive indices of the sheared solution parallel to O*x* axis and O*z* axis and sample thickness, respectively. Time changes in scattered light intensity parallel $I_{\parallel}(q_1,t)$ and perpendicular $I_{\perp}(q_1,t)$ to flow were simultaneously measured by a set of small photodiodes (part 7) in the O*xz* plane, as shown in Figure 1d. An effective area of the photodiode used was 1 mm^2, and the corresponding q value q_x or q_z is $q_1 = q_x = q_z = (3.34 \pm 0.13) \times 10^{-4}$ nm^{-1}.

Time dependence of shear stress σ and first normal stress difference N_1 after onset of shear flow were measured by ARES (TA Instruments, New Castle, DE) with a cone and plate fixture (25 mm diameter and cone angle is 0.1 rad).

III. Experimental Results

III-1. Time Evolution of Shear-Induced Structure after Step-Up Shear Flow. III-1-a. Shear SALS. Shear flow at a given shear rate was imposed on the solution at time $t = 0$ s, and a constant shear rate was kept before shear cessation. Time change in scattering pattern was recorded by the CCD camera. The incident beam has a polarization direction parallel to the O*z* axis, and the analyzer was not used between sample and the detector. Hence, the light scattering pattern shown in this section arises from both fluctuations of refractive index and optical anisotropy, since the scattered intensity is a sum of V_H and H_H scattering under this condition where the vertical direction was set along the O*x* axis.[21,22]

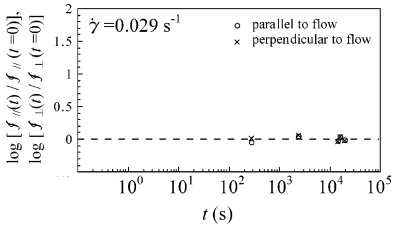

Figure 2. Time change in the reduced integrated scattered intensity parallel and perpendicular to flow axis after imposing the step-up shear flow from zero shear rate to a shear rate of 0.029 s^{-1} in regime I.

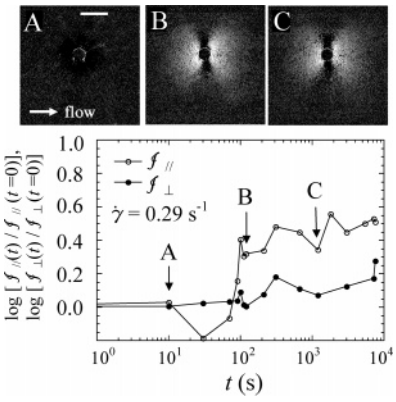

Figure 3. Time evolution of scattering patterns, which were taken at (A) 10 s, (B) 120 s, and (C) 1200 s, and the reduced integrated scattered intensity $\mathcal{J}_{\perp}$ and $\mathcal{J}_{\parallel}$ after imposing the step-up shear flow from zero shear rate to a shear rate of 0.29 s^{-1} in regime II. In the bottom plot, the arrows marked by A, B, and C indicate the time when the top patterns A to C were taken. Scale bar inserted in pattern A is $q = 5.2 \times 10^{-4}$ nm^{-1}, and this can be commonly used for the patterns B and C. The flow direction is also common for the patterns A to C (in horizontal direction).

We shall describe below the time evolution of the shear-induced structures after the step-up shear into various shear regimes, i.e., regime I to regime III defined in section I.

Step-Up Shear into Regime I. Figure 2 shows the time change in reduced integrated scattered intensity $\mathcal{J}_{\parallel}$ and $\mathcal{J}_{\perp}$ under the shear flow after onset of step-up shear to $\dot{\gamma}$ of 0.029 s^{-1} in regime I. The reduced integrated intensity was obtained by normalizing the integrated intensity under flow with that at quiescent state $\mathcal{J}_{\parallel}(t = 0)$ or $\mathcal{J}_{\perp}(t = 0)$. The scattered intensity under the shear flow is very weak in both directions and kept the same value as that of the quiescent state. At this shear rate, shear-induced structure was not developed, and the concentration fluctuations are essentially identical to those of homogeneous semidilute solutions.

Step-Up Shear into Regime II. After imposing the step-up shear from zero shear rate to 0.29 s^{-1} in regime II, the characteristic scattering pattern was developed as shown by patterns A to C in Figure 3. Scattered intensity was high parallel to the flow direction and weak in perpendicular direction. This characteristic scattering pattern has been designated as the "butterfly pattern" which is characteristic for shear-induced concentration fluctuations and/or phase separation.[23,24] The bottom part in Figure 3 shows time changes in the $\mathcal{J}_{\parallel}$ and $\mathcal{J}_{\perp}$ after onset of the shear flow. During several tens of seconds, the scattered intensities kept same value as that of quiescent state. After this incubation time of

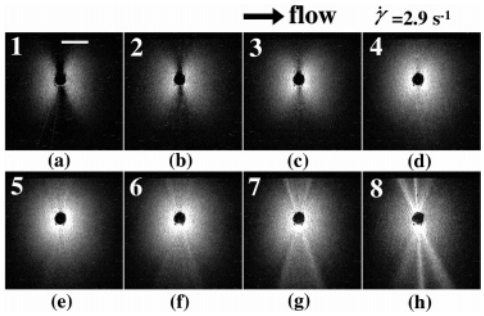

Figure 4. Time change in scattering pattern after imposing the step-up shear flow from zero shear rate to a shear rate of 2.9 s^{-1} in regime III. Time elapsed after the onset of the shear flow is (a) 5, (b) 55, (c) 70, (d) 90, (e) 100, (f) 120, (g) 150, and (h) 240 s. The numbers from (1) to (8) inserted in the figure are consistently used in this paper to refer particular times after onset of the shear at $\dot{\gamma}$ = 2.9 s^{-1}. Scale bar which is inserted in the in part (a) is $q = 5.2 \times 10^{-4}$ nm^{-1} and is commonly used to other scattering patterns.

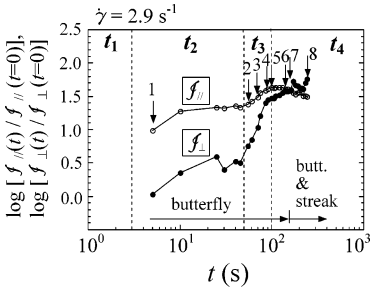

Figure 5. Time change in integrated scattered intensity after imposing the step-up shear flow from zero shear rate to 2.9 s^{-1}. The numbers (1) to (8) inserted in the figure correspond to the numbers in Figure 4. The vertical lines correspond to those in Figure 8 to be shown later for classification of time regions to characterize the transient changes in birefringence and scattered intensity.

about a hundred seconds, $\mathcal{J}_{||}$ began to increase. The scattered intensity reached a constant level and held the same intensity over several hours. The scattered intensity perpendicular to the flow kept almost the same value as or slightly higher than that from quiescent solution throughout this experiment.

Step-Up Shear into Regime III. Figure 4 shows the time change in scattering pattern after imposing the step-up shear of shear rate 2.9 s^{-1} in regime III. The scattering patterns in parts a and b of Figure 4 taken at 5 and 55 s after onset of the shear flow shows the butterfly pattern. The scattered intensity became strong and the dark streak became narrow with time. From t = 70 to 100 s (Figure 4c−e), the scattered intensity perpendicular to shear flow became stronger so that the dark streak became ambiguous. At t = 120 s (Figure 4f), a weak but obvious streak pattern appeared approximately along the Oz axis. As time further elapses, the streak pattern became stronger (Figure 4g,h).

Figure 5 shows the time change in the reduced integrated scattered intensity at $\dot{\gamma} = 2.9$ s^{-1}. At $t = 5$ s, $\mathcal{J}_{||}$ increased to a value which is 10 times as large as that for quiescent state, though $\mathcal{J}_\perp$ kept the same value as that from quiescent. The incubation time for the appearance of the butterfly patterns become shorter than 5 s, much shorter than the step-up shear into regime II (Figure 3). In the time interval from 10 to 50 s, $\mathcal{J}_{||}$ reached a constant value, whereas $\mathcal{J}_\perp$ gradually increased which may imply shear-induced phase separation.[24] At t > 60 s, $\mathcal{J}_{||}$ began to increase again, and

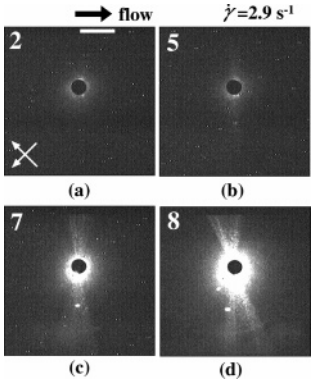

Figure 6. Cross-polarized small-angle light scattering pattern under shear flow at shear rate of 2.9 s^{-1}. Time elapsed after onset of the step-up shear flow is (a) 55, (b) 100, (c) 150, and (d) 240 s. The numbers indicated in the figure correspond to the numbers in Figure 4. Flow direction is horizontal in this figure. The bright scale bar inserted in Figure 6a is $q = 5.2 \times 10^{-4}$ $nm^{-1}$and is common for other patterns. The bright arrows indicate the polarization directions of polarizer and analyzer.

$\mathcal{J}_\perp$ increased more steeply than $\mathcal{J}_{||}$. In the time interval from 60 to 110 s where the scattering patterns corresponding to 3−5 in Figure 4 are observed, $\mathcal{J}_\perp$ increased steeply, although the scattering patterns are diffuse and streak pattern still not appeared. At t = 120 s (number 6), the streak pattern became visible as shown in Figure 4f. Beyond this time, the $\mathcal{J}_{||}$ turned into decrease, whereas the streak pattern became stronger so that $\mathcal{J}_\perp > \mathcal{J}_{||}$. The time evolution of scattering can be classified into four regions, t_1 to t_4, as shown in Figure 5. The time regions defined are also consistent with the time change in birefringence as will be shown later in section III-1-c. The detailed discussion about this classification will be deferred until section IV later.

Small-angle light scattering under cross-polarization will give us information about optical anisotropy of shear-induced structure. We performed the scattering experiment under the cross-polarization after the onset of step-up shear. Figure 6 shows the time change in the scattering patterns obtained under cross-polarization. At the time when only the butterfly pattern was developed as shown in Figure 4b (pattern 2), the scattering under the cross-polarization was very weak (Figure 6a). It means that only the concentration fluctuations but no optical anisotropy developed at this moment. At t = 100 s (Figure 6b), the scattered intensity under cross-polarization became stronger only perpendicular to the flow, whereas the scattered intensity parallel to flow kept almost the same intensity level as that at quiescent, although the trend may not be easily discerned in the figure. This means that the optical anisotropy fluctuations were developed at this time, and the correlated fluctuations would extend in the direction parallel to the flow. At the time scale longer than 120 s (Figure 6c,d), the scattered intensity under the cross-polarization became stronger in the direction perpendicular to flow and the streak pattern obviously developed. This clearly indicates that the structure giving rise to the streak pattern in SALS shown in Figure 4g,h has optical anisotropy.

III-1-b. Shear Microscopy. Step-Up Shear into Regimes I and II. There are no shear-induced structures as observed under shear microscopy after the step-up shear into regime I ($\dot{\gamma} = 0.029$ s^{-1}). This is consistent with the shear SALS result. The step-up shear into regime II ($\dot{\gamma} = 0.29$ s^{-1}) exhibited shear-induced struc-

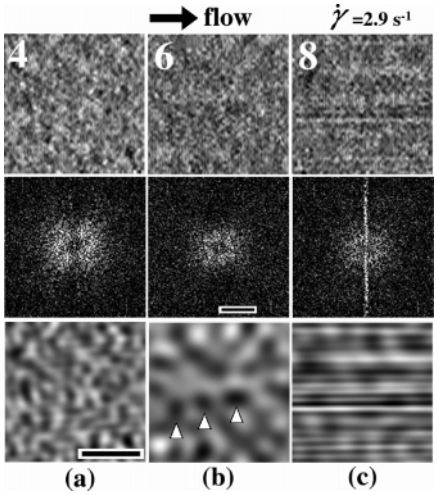

Figure 7. Shear microscopy at shear rate of 2.9 s^{-1} in regime III. Time elapsed after imposing step-up shear from zero shear rate to 2.9 s^{-1} is (a) 90, (b) 120, and (c) 240 s. The numbers indicated in the figure correspond to the numbers in Figure 4. Flow direction is horizontal in this figure. Top images are the original micrographs. Middle patterns are the 2D-FFT spectra calculated from the original images. Bottom images are the filtered images which enhance the flow-induced structures. Procedure of the image filtering is depicted later in Figure 14. Scale bars inserted in the middle pattern and the bottom image are 0.1 μm^{-1} and 50 μm, respectively, and are commonly used for other FFT spectrum and optical images, respectively. Three white triangles in the bottom picture of (b) indicate an assembly of domains observed in this time region.

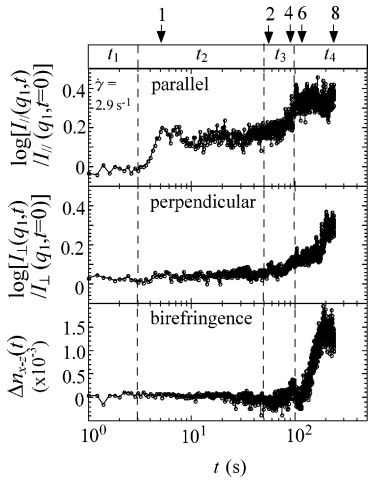

Figure 8. Time change in shear birefringence and simultaneously measured scattered intensity as a function of elapsed time after imposing the step-up shear from zero shear rate to 2.9 s^{-1} in regime III. Top and middle parts of the figures are the scattered intensity parallel and perpendicular to the flow at $q = (3.34 \pm 0.13) \times 10^{-4}$ nm^{-1}, respectively. Bottom is shear birefringence. Numbers on top of the figure correspond to those in Figure 4.

ture under shear microscopy after the same incubation period as that found for the corresponding shear SALS experiment. The shear-induced structure observed was essentially the same as that found previously for the same solution at 150 °C and at $\dot{\gamma} = 4.6$ s^{-1} (see Figure 6 in ref 9).

Step-Up Shear into Regime III. Figure 7 shows the results of shear microscopy under the same condition as that used for the light scattering experiment. The top series of Figure 7 is the original micrograph taken under the shear flow. The middle part is the spectra of two-dimensional fast Fourier transform (2D-FFT) of the original micrograph. The bottom part is the filtered images calculated by the computer to enhance the real space image responsible for the butterfly plus the streaklike scattering pattern (see Appendix for details).

At 90 s after the shear start (Figure 7a), "ripple-like" contrast fluctuations between dark and bright, which appear to be elongating perpendicular to the flow, was observed in the optical micrograph. This "ripples" must correspond to the structure giving rise to the butterfly pattern shown in Figure 4c,d (patterns 3 and 4) because the 2D-FFT of the micrograph shows the butterfly-type pattern, as shown in the middle pattern in Figure 7a. In the SALS pattern (Figure 4d), $\mathcal{J}_\perp$ (Figure 5) was about 30 times higher than that of quiescent solution. We believe that the increase in the scattered intensity perpendicular to the flow in SALS should indicate a trend toward formation of an assembly of polymer-rich domains along flow. The detailed discussion about the structure will be given later in this paper in conjunction with an experiment of light scattering and microscopy after shear cessation.

The spatial frequency of the "ripples" along the flow direction looks to decrease with time ($t = 120$ s, Figure 7b). Corresponding to this change, the 2D-FFT pattern of the micrograph shown in middle of Figure 7b exhibits the following changes: shrinkage of butterfly-type pattern to lower frequency (longer characteristic length) and an increase of the intensity of the spectrum perpendicular to the flow, which makes the butterfly-type pattern ambiguous. The filtered image in the bottom of Figure 7b shows a contrast fluctuation having a longer characteristic length than that of Figure 7a. Moreover, it is noteworthy that an assembly of dark regions was observed in the figure as indicated by white triangles. We believe that the assembly gives rise to an assembly of bright regions in its next neighbor and that these assemblies aligned approximately parallel to the flow direction are responsible for the increase of the intensity perpendicular to flow in the FFT spectrum.

At $t = 240$ s (Figure 7c), many fibrous structures elongated parallel to the flow were observed in the bottom of Figure 7c. From the resemblance of the streak pattern in shear SALS shown in Figure 4g,h with that of 2D-FFT spectrum in the shear microscopy (middle pattern in Figure 7c), it is clear that the fibrous structure shown in the bottom of Figure 7c corresponds to the structure giving rise to the streak pattern in shear SALS in Figure 4g,h.

III-1-c. Shear Birefringence. We performed a simultaneous experiment for shear SALS at particular q's and shear birefringence to elucidate the detailed relationship between the development of the scattered intensity and birefringence. Since we observed a significant signal of birefringence only in regime III, we shall present here only the step-up shear experiments to a shear rate of 2.9 s^{-1}. Figure 8 shows time change in the small-angle scattered intensity at a particular value of $q_1 = (3.34 \pm 0.13) \times 10^{-4}$ nm^{-1} and time change in birefringence. The four time regions as already shown in Figure 5 are also included here. In time region t_1 (incubation period), where the elapsed time from shear start is less than 3 s, the scattered intensity kept the same value as that of quiescent solution. Here the birefringence is also kept zero, so that the sheared solution is optically isotropic as in a quiescent solution. In time region t_2 ($3 \leq t \leq 50$ s, period for the shear-

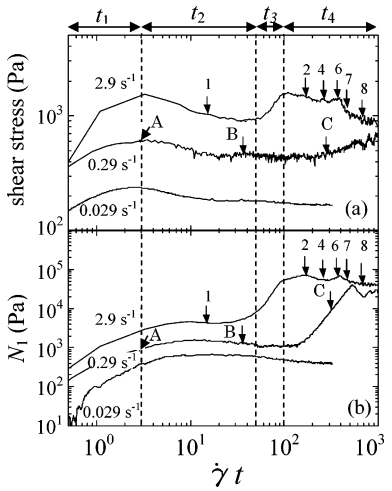

Figure 9. Time change in (a) shear stress σ and (b) first normal stress difference N_1 as a function of $\dot{\gamma}t$ after imposing the step-up shear from zero shear rate to given shear rates. The inserted letters and numbers in the figure correspond to those in Figures 3 and 4, respectively.

induced concentration fluctuations being developed) the scattered intensity parallel to flow increased and subsequently reached a plateau value, whereas the intensity perpendicular to the flow and birefringence kept constant values nearly equal to the values in quiescent state. As shown in Figures 4 and 5, only the butterfly pattern is developed in this region. At times longer than 50 s, the scattered intensity parallel to flow began to further increase with time, and the scattered intensity perpendicular to flow also started increasing (time region t_3 for the precursory period for shear-induced crystallization). The birefringence still kept zero as in a quiescent solution. In the time region t_4 ($100 \leq t \leq 240$ s, period for shear-induced crystallization) the birefringence and the intensity perpendicular to flow increased drastically, while the intensity parallel to flow reached another plateau value. The structures developed in the solution in each region will be discussed later in section IV.

III-2. Time Evolution of Shear Stress and Normal Stress Difference under Shear Flow. Here we focus on the development of shear stress and normal stress difference, and we would like to discuss about the relationship between time evolution of the stress and the scattering or shear-induced structures after onset of the step-up shear.

The imposed shear rates to be discussed here are 0.029, 0.29, and 2.9 s^{-1}, belonging to regimes I, II, and III, respectively. Figure 9 shows time evolution of the shear stress σ (part a) and the first normal stress difference N_1 (part b) after onset of the shear flow at the given constant shear rates. The vertical broken lines indicate the same boundaries of the time regions as those designated for time evolutions of shear light scattering and shear birefringence. At the lowest shear rate, $\dot{\gamma} = 0.029$ s^{-1} in regime I, both σ and N_1 show a very weak overshoot. The shear stress σ instantaneously began to increase at onset of the shear flow and increased toward stress maximum at $\dot{\gamma}t \cong 3$. Then the shear stress turned into a decrease and reached asymptotically a constant value at around $\dot{\gamma}t = 15$. N_1 reaches the maximum at $\dot{\gamma}t \cong 10$, at a time longer than σ. At shear rate of 0.29 s^{-1} in regime II, both σ and N_1 also showed the first overshoot. Evolution of the first overshoot of σ and N_1 as a function of $\dot{\gamma}t$ is almost same as that of 0.029 s^{-1}. On the contrary to $\dot{\gamma} = 0.029$ s^{-1}, the σ and N_1 at $\dot{\gamma} = 0.29$ s^{-1} increased after the first overshoot. This increase may indicate onset of the second overshoot. N_1 remarkably increased more than one decade starting at $\dot{\gamma}t = 100$ after onset of the first overshoot. At the highest shear rate of 2.9 s^{-1}, in regime III, the second stress overshoot was more clearly observed. The values $\dot{\gamma}t$ of the peak top for the first overshoot were almost same in all shear regimes, equal to 3 for σ and 10 for N_1; hence, the first overshoot of shear stress occurs prior to that of N_1 in all shear regimes. On the other hand, the strain $\dot{\gamma}t$ for the onset of the second overshoot was observed to become smaller with increase shear rate, in both σ and N_1.

To elucidate a relationship between development of the stresses and that of the structures observed by the light scattering, one should note that numbers 1−8 and letters A−C in Figure 9 correspond to the scattering patterns A−C in Figure 3 for $\dot{\gamma} = 0.29$ s^{-1} and those 1−8 in Figure 4 for $\dot{\gamma} = 2.9$ s^{-1}. At shear rate of 0.29 s^{-1} (regime II), the following points are worth noting. At the peak top of the first overshoot of σ (part a, $\dot{\gamma}t = 3$) the butterfly pattern cannot be clearly observed in the Oxz plane, as shown in pattern A of Figure 3. The butterfly pattern shown in pattern B in Figure 3 is seen to develop nearly after the end of the first overshoot of σ (B in Figure 9). This trend is identical to those observed for the non-crystallizable semidilute solution of PS/DOP,[19] indicating that the first stress overshoot is followed by the development of concentration fluctuations enhanced by shear flow. At shear rate of 2.9 s^{-1} (regime III), almost the same trend as that at 0.29 s^{-1} was discerned with respect to the first overshoot of σ and N_1. However, comparisons between the stresses and scattering patterns lead to finding the following new piece of evidence in PE solution which cannot be found with PS/DOP. At $\dot{\gamma}t$ of 435 and 696 which are indicated by the arrows with numbers 7 and 8, the streak pattern with optical anisotropy began to develop as shown in Figure 6c,d after nearly the end of the second overshoot and beginning of the third overshoot in σ and N_1. Therefore, the second stress overshoot appears to be followed by the development of fibrous crystalline structure.

III-3. Time Change in Scattered Intensity after Cessation of Shear Flow. Figure 10 shows the time change in scattering pattern obtained after cessation of shear at 2.9 s^{-1}: The shear flow was ceased at $t = 95$ s (t_3 region) after onset of the step-up shear at 2.9 s^{-1}. As clearly suggested from Figures 4 and 5, the distinct streak pattern in SALS is not observed yet at the time when the shear flow is ceased, as it should appeared at $t = 150-240$ s (patterns 7 and 8 in Figure 4). It should be recalled that in this time region the scattered intensity perpendicular to flow gradually increased, whereas the birefringence kept nearly zero. At 90 s after onset of the step-up shear but immediately before the cessation (pattern a), the pattern is butterfly type, but the dark streak looks obscured because the streak pattern appeared normal to flow with a weak scattered intensity seemingly overlapped to the strong butterfly pattern. At 5 s after the cessation (pattern b) the butterfly pattern decayed very quickly. The scattered intensity perpendicular to flow also decayed; however, the decay rate slowed down with time, and it turned into an increase. At $t = 180$ s after the cessation (pattern c) a weak but discrete streak pattern was observed. The

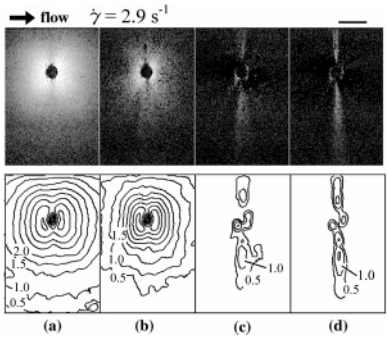

Figure 10. Time change in scattering patterns before and after cessation of the shear at shear rate of 2.9 s^{-1}. The shear flow was ceased at 95 s in time region t_3 after imposing the step-up shear from zero shear rate to 2.9 s^{-1}. Top pictures are the scattering patterns and bottom pictures are the contour plots of each scattering patterns which were taken at t = (a) 90 (before the cessation), (b) 100, (c) 275, and (d) 1895 s after the onset of the step-up shear. The scale bar which is shown on the top of (d) corresponds to $q = 5.2 \times 10^{-4}$ nm^{-1} and is commonly used for other scattering patterns and contour patterns.

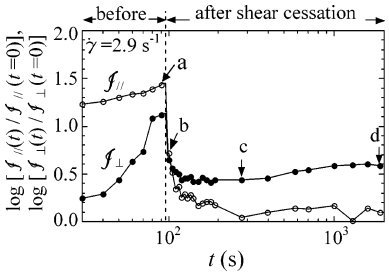

Figure 11. Time change in the integrated scattered intensity as a function of time t elapsed after the onset of the step-up shear from zero shear rate to a shear rate of 2.9 s^{-1}. The shear flow was ceased at t = 95 s. The integrated scattered intensities parallel and perpendicular to flow were normalized with that of quiescent solution. The letters a to d in the figure correspond to times at which the patterns (a) to (d) in Figure 10 were observed.

intensity of the streak pattern increased with time as shown in Figure 10d. The time changing in the scattered intensity parallel and perpendicular to flow is more quantitatively presented in Figure 11.

Figure 12 shows the time change in transmission optical image obtained after cessation of shear at the same condition as in Figure 10. At t = 90 s immediately before the cessation (Figure 12a), the FFT spectrum numerically calculated from the micrograph shows a butterfly-type pattern. However, the dark streak of the spectrum is ambiguous, in consistent with the SALS pattern in Figure 10a. The bottom series of Figure 12 is the filtered images. Dark and bright contrast elongating perpendicular to the flow (ripplelike contrast) is observed in the figures. It should be noticed that a stringlike assembly of the dark and bright clusterlike regions oriented parallel to the flow is observed in Figure 12a,b (indicated by black triangles). At t = 100 s (5 s after the cessation, Figure 12b), the butterfly-type pattern in FFT spectrum shrank to a smaller q, and the streak-type pattern became more obvious than that of Figure 12a, both consistent with Figure 10b. With increasing time after the cessation, the streaklike scattering pattern and hence fibrous structures became clearer as shown in the filtered images, and the butterfly pattern degenerated into a small q-limit, indicating characteristic length of ripplelike contrast became

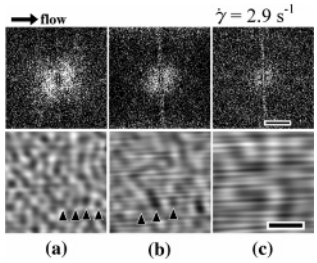

Figure 12. Time change in optical microscope images before and after cessation of the shear at shear rate of 2.9 s^{-1}. The shear flow was ceased at 95 s in time region t_3 after onset of the shear start as in the case of Figure 10. Top patterns are the 2D-FFT spectra numerically calculated from original micrographs and bottom images are the filtered images calculated from the original image based on the procedure as depicted in Figure 14. These patterns and images were taken at t = (a) 90 (before the cessation), (b) 100, and (c) 110 s after onset of the shear. Scale bars on the top and bottom patterns of part c correspond to 0.1 μm^{-1} and 50 μm, respectively, and are commonly used to other FFT spectra and filtered images, respectively. Black arrows inserted in the bottom pictures in parts a and b indicate an assembly of domains aligned parallel to flow.

larger. The results are consistent with those in Figure 10c,d.

IV. Discussion

IV-1. Classification of Time Evolution of Shear-Induced Structures after Step-Up Increase of Shear Rate into Shear Regime I to III. For the case of the step-up shear to a shear rate in regime I ($\dot{\gamma} < \dot{\gamma}_{c,butterfly}$), the solution under shear flow remains the same state as the quiescent solution, as clarified from the results in section III (Figure 2). No shear-induced structures were observed under shear microscopy, and the sheared solution did not show any birefringence.

For the case of the step-up shear into regime II ($\dot{\gamma}_{c,butterfly} < \dot{\gamma} < \dot{\gamma}_{c,streak}$), the butterfly pattern was developed after an incubation time and reached a steady state pattern under the shear flow (Figure 3). No birefringence was observed, but the shear-induced optically isotropic structures were observed after the incubation period.

For the case of the step-up shear into regime III ($\dot{\gamma} > \dot{\gamma}_{c,streak}$), after an incubation time (**time region t_1**) the butterfly pattern was developed at first (**time region t_2**) (Figures 4a and 5). Here optically isotropic, phase-separated domain structures are developed.[9] The domains being optically isotropic were confirmed by no appreciable scattered intensity under cross-polarizers. The domains are expected to be elongated normal to the flow axis, judging from the compressed shape of the butterfly pattern with respect to flow axis (Figure 4a). The domains centers are also expect to be randomly distributed with respect to flow axis and the neutral axis, which is inferred from the result shown in Figure 7a. After the scattered intensities $\mathcal{J}_{\perp}$ and $\mathcal{J}_{||}$ reached steady values (Figure 5, **time region t_4**), the optically anisotropic streaklike pattern was developed perpendicular to the shear flow (Figure 6c,d) in addition to the butterfly pattern (Figure 4f–h). Here domains tend to align parallel to flow axis to form stringlike assemblies (Figure 7e), giving rise to an optically anisotropic fibrous texture (Figure 8).

We shall defer the discussion of the time region t_3 until later in section IV-2 and continue further to discuss the time region t_4. We can propose that this

optically anisotropic fibrous texture is crystalline by the following piecies of evidence: (1) The previous result on time changes of the steady-state streak pattern (as shown in Figures 4f,g and 6c,d) after the cessation of shear showed that the streak pattern remained even after the cessation (Figure 9 of ref 10), supporting formation of shear-induced formation of crystalline fibrous texture. If it is not crystallized, the fibrous structure will disappear after the cessation. (2) The streak pattern was observed under cross-polarization (Figure 6c,d), indicative of the structure having an optical anisotropy. (3) A steep increase of birefringence coincided with the development of the streak pattern (Figure 8), indicative of the domains aligned into string or fibril and connected together by highly oriented chains.

All the characteristic features in time change in the shear-induced structures after the step-up shear into regime III, as elucidated from the results shown in Figures 4−12, highlight the development of shear-induced phase separation prior to the crystallization. This phase separation must cause the following effect on crystallization; the crystallization should be enhanced or triggered locally in the regions rich in polymer. This is because those regions rich in polymer concentration have a higher melting temperature than that for the solution with the average concentration and hence a higher degree of supercooling. Those regions should bear a larger stress level than the counterpart regions, which may eventually trigger stress-induced chain orientation in the string. We shall give the more detailed discussion concerning the relation between the crystallization and the phase separation in the next section.

IV-2. Relationship between Development of Butterfly Pattern and That of Streak Pattern. The bright streak perpendicular to shear flow is not a unique characteristic observed only for the polyethylene solutions, but it was also observed in the noncrystallizable (atactic) polystyrene (PS) solutions at shear rates higher than critical shear rate $\dot{\gamma}_a$.[25] Origin of the bright streak in the polystyrene solutions is proposed to be assemblies of polymer-rich domains aligned in the direction parallel to the shear flow defined as "stringlike domain structure". In this shear regime (corresponding to regime IV in the case of the PS solutions[25,26]), the solutions showed a large negative birefringence (and hence a high degree of chain orientation parallel to shear flow[27]). Thus, the domains in the string seem to be connected each other with highly oriented chains. Form dichroism exhibited a large positive value, consistent with assemblies of polymer-rich domains into strings parallel to flow direction.[26−28] Moreover, at the higher shear rates in regime IV, shear stress and the first normal stress difference were abnormally increased.[25] Thus, even in the case of the noncrystallizable semidilute solutions of PS, the optically anisotropic fibrous structures are formed. However, they are not crystallized and kept essentially in **shear-induced oriented nematic states**. Hence, they are relaxed completely into isotropic solutions after cessation of the shear. In the case of the UHMWPE solution **nematically oriented chains will be spontaneously crystallized** so that anisotropic fibrils can exist even after cessation of the shear. In this section, let us discuss the experimental results obtained in the polyethylene solutions from the point of view of the string phase commonly developed for sheared solutions of both noncrystallizable and crystallizable polymers.

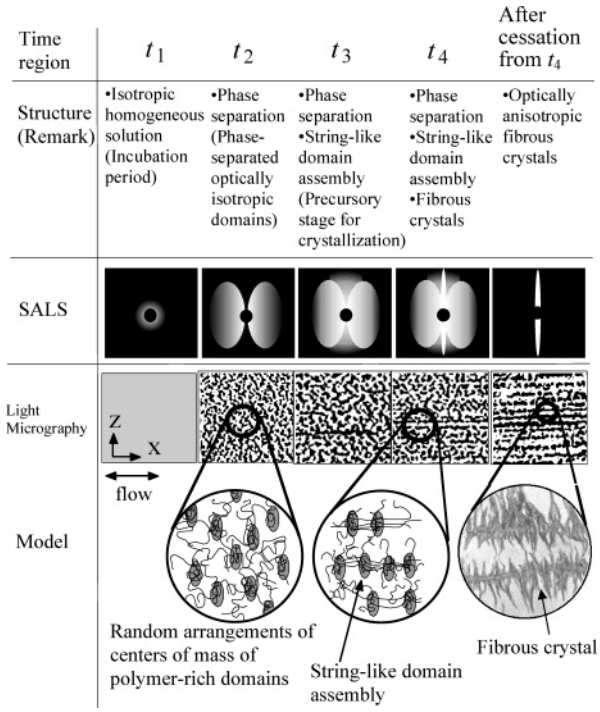

Figure 13. Schematic representation of time evolutions of the SALS and shear-induced structures after a step-up increase of shear rate from zero shear rate to a shear rate higher than the critical shear rate of streak pattern (regime III).

At the boundary of the shear regime III (butterfly) and IV (stringlike structure) in PS solutions, a steep change in birefringence from nearly zero to a large negative value was observed.[27] In the case of polyethylene solution, a steep increase of birefringence from nearly zero to a large positive value was observed in synchronization with development of the streak pattern in regime III, as a consequence of regime III and regime IV being degenerated in the UHMWPE solutions as clarified in our previous paper.[10] This fact clearly elucidates that crystallizability of UHMWPE strongly promote formation of optically anisotropic fibrous (or string) structure.

Let us look at the time change in light scattering and birefringence from the UHMWPE solutions in detail after the step-up shear into regime III. In **time region t_3** defined in Figures 5, 8, and 9, scattered intensity perpendicular to shear flow began to increase, whereas the birefringence kept approximately zero value. Therefore, the contribution of the optical anisotropy to the increment of scattered intensity must be small. This is consistent with the results shown in Figure 6a,b. Thus, the stringlike structure in time region t_3 may be considered as a precursor for formation of optically anisotropic fibrous crystalline structures parallel to flow in time region t_4.

We already showed that the butterfly-type scattered intensity quickly decayed after cessation of shear at time region t_3 (see results shown in Figure 10). This strongly indicates that the dominant structure giving rise to the scattered intensity perpendicular to flow in this time region (t = 95 s in Figure 11) must be that giving rise to the concentration heterogeneities (optically isotropic phase-separated domains aligned into stringlike precursory structure; see the model for stringlike domain assembly to be discussed in Figure 13 later) aligned

parallel to flow. Moreover, we realize that a small fraction of crystalline fibrous structure should be already developed in this time region, as unveiled from the fact that the streaklike scattering pattern, indicative of the fibrous or stringlike structures, is conserved even at a long time after cessation, as shown in Figures 10 and 11. This is simply because the fibrous structures would not be dissolved and decayed even after the shear cessation, if they were crystallized. They would decay, if they were not crystallized as in the case of the sheared PS solutions. This means that a minor fraction of the precursory stringlike structure may be already transformed into the fibrous crystalline structure. However, at this stage the precursory structure does not show a significant amount of birefringence. The corresponding scattering was not clearly resolved before the cessation as it is overwhelmed by the butterfly scattering.

We propose a schematic model in Figure 13 which summarizes the time evolution of shear-induced structures as observed by the transient changes in shear SALS, shear microscopy, and shear birefringence after a step-up shear from zero shear rate to a given shear rate in regime III. Time regions t_1 to t_4 are those defined in Figures 5, 8, and 9. In time region t_1 (incubation period for shear-induced structure formation) the solution keeps the same state as quiescent solution. In time region t_2 the phase separation is induced by the flow, and the butterfly pattern is developed in SALS. Here polymer-rich regions (e.g., dark region in light microscopy) extended along the neutral direction, but their centers of mass are randomly distributed along neutral direction (Oz axis) and along flow axis. In time region t_3, the scattered intensity perpendicular to flow begins to increase due to self-assembly of polymer-rich domains parallel to the flow axis. This structure may be considered as a precursory structure for the stringlike domains parallel to flow. A partial crystallization into fibrous crystalline structure may occur, but the precursory structure does not show an appreciable value of birefringence yet. In time region t_4, the well-defined stringlike structure aligned parallel to flow axis will be formed. At the same time molecular orientation increases, optically anisotropic fibrous crystalline texture (or string) grows, and an optical anisotropic streak pattern clearly develops. After the shear cessation the fibrous crystals remains, whereas the butterfly pattern disappears, probably because the domains tend to be transformed into the fibrils. The fibrous crystals remained after the cessation is expected to be the shish-kebab structure, as schematically illustrated in the right edge in Figure 13, the confirmation of which deserves future works.

V. Summaries

The shear-induced structure of ultrahigh molecular weight polyethylene (UHMWPE) was investigated, in situ and at real time, with shear small-angle light scattering, shear microscopy, birefringence, and rheology. We conducted the experiments at temperature of 124 °C, which is approximately equal to the equilibrium melting temperature but higher than the highest nominal melting temperature (118 °C) of crystals in the quiescent solution.

Upon imposing a step-up shear from zero shear rate to a shear rate higher than $\dot{\gamma}_{c,streak}$ in regime III, the butterfly pattern was developed prior to the streak pattern. From the careful comparison between time

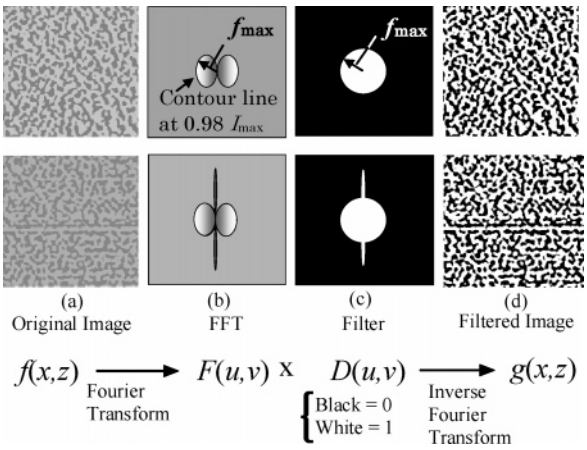

Figure 14. Schematic representation of the image filtering process to obtain the bottom three images in Figures 7 and 10. Original real space image $f(x,z)$, either for the image at the top or bottom in part (a) was transformed into Fourier-space image by two-dimensional fast Fourier transform (2D-FFT) to obtain $F(u,v)$. Next, the Fourier space image $F(u,v)$ was multiplied by a spatial filter $D(u,v)$ (shown by part c), and the product $F(u,v)D(u,v)$ was transformed into real space image $g(x,z)$ by inverse 2D-FFT (part d). The detailed procedure is presented in the text.

change in scattered intensity and birefringence after application of the step-up shear, it was elucidated that the stringlike assembly of domains parallel to the flow as observed in the PS/DOP systems were developed, and this precursory structure may trigger crystallization into optically anisotropic fibrous structures for the cases of crystallizable polymers.

The scattering pattern exhibited both the "butterfly" scattering pattern and the "streak" scattering pattern in time region t_4. The butterfly pattern had the following characteristics: it cannot be observed under cross polarizers, and it disappears after cessation of the shear. These characteristics suggest that the pattern arises from shear-enhanced concentration fluctuations or shear-induced liquid−liquid phase separation and that the domains responsible for the butterfly pattern are still optically isotropic. As for the streak scattering we note the following: it can be observed under crossed polarizations, suggesting that it arises from optically anisotropic fibrous structure aligning along the flow direction. The structural entity was supported also by shear microscopy. In the anisotropic fibrous stringlike structures, the domains are interconnected with highly oriented chains.

Appendix

At first, the original image $f(x,z)$ (part a) was transformed into the Fourier space to obtain $F(u,v)$ where u and v are horizontal and vertical spatial frequencies (part b), respectively. Next, the function $F(u,v)$ was filtered by multiplying with a filter function $D(u,v)$ (part c). To obtain the filter function, $F(u,v)$ was smoothed, and a contour line with an isointensity level of $0.98I_{max}$ was constructed from the smoothed spectrum defined by $F^s(u,v)$, where I_{max} is the maximum intensity of $F^s(u,v)$. From the contour line, a characteristic spatial frequency (defined as f_{max}) was obtained. We created the filter function $D(u,v)$ which was set to 1, if $(u^2 + v^2)^{0.5} \leq f_{max}$ and 0 if $(u^2 + v^2)^{0.5} > f_{max}$. If the FFT spectrum shows a streak pattern as in the case of a bottom half of Figure 14b, we add a filter function corresponding to the streak-type pattern to $D(u,v)$. Finally, a filtered real-

space image $g(x,z)$ was reconstructed from the filtered function $F(u,v)D(u,v)$ through inverse FFT. In such image processing we can extract and enhance the structure giving rise to the butterfly- and streak-type spectrum from the original image.

References and Notes

(1) Ver Strate, G.; Phillipoff, W. *J. Polym. Sci., Polym. Lett. Ed.* **1974**, *12*, 267.
(2) Schumidt, R. J.; Wolf, B. A. *Colloid Polym. Sci.* **1979**, *257*, 1188.
(3) Rangel-Nafaile, C.; Metzner, A. B.; Wissbrun, K. F. *Macromolecules* **1984**, *17*, 1187.
(4) Helfand, E.; Fredrickson, G. H. *Phys. Rev. Lett.* **1989**, *62*, 2468.
(5) Onuki, A. *Phys. Rev. Lett.* **1989**, *62*, 2472, *J. Phys.: Condens. Matter* **1997**, *9*, 6119.
(6) Milner, S. T. *Phys. Rev. E* **1993**, *48*, 3674.
(7) Doi, M.; Onuki, A. *J. Phys. II* **1992**, *2*, 1631.
(8) Onuki, A. In *Phase Transition Dynamics*; Cambridge University Press: Cambridge, UK, 2002.
(9) Murase, H.; Kume, T.; Hashimoto, T.; Ohta, Y.; Mizukami, T. *Macromolecules* **1995**, *28*, 7724.
(10) Murase, H.; Kume, T.; Ohta, Y.; Hashimoto, T. *Macromolecules* **2005**, *38*, 6656.
(11) Pennings, A. J.; Kiel, A. M. *Kolloid Z. Z. Polym.* **1965**, *205*, 160.
(12) Keller, A.; Machin, M. J. *J. Macromol. Sci., Phys.* **1967**, *B1*, 41.
(13) Rietveld, J.; McHugh, A. J. *J. Polym. Sci., Polym. Phys. Ed.* **1985**, *23*, 2339.
(14) McHugh, A. J.; Rietveld, J. *J. Polym. Sci., Polym. Phys. Ed.* **1985**, *23*, 2359.
(15) McHugh, A. J.; Spevacek, J. A. *J. Polym. Sci., Part B: Polym. Phys.* **1991**, *29*, 969.
(16) McHugh, A. J.; Edwards, B. J. In *Rheo-Physics of Multiphase Polymeric Systems*; Lyngaae-Jørgensen, J., Søndergaard, K., Eds.; Technomic Publishing: Lancaster, PA, 1995; Chapter 5.
(17) McHugh, A. J. In *Rheo-Physics of Multiphase Polymeric Systems*; Lyngaae-Jørgensen, J., Søndergaard, K., Eds.; Technomic Publishing: Lancaster, PA, 1995; Chapter 6.
(18) Hoffman, J. D.; Weeks, J. J. *J. Res. Natl. Inst. Stand. A: Phys. Chem.* **1962**, *66A*, 13.
(19) Kume, T.; Hattori, T.; Hashimoto, T. *Macromolecules* **1997**, *30*, 427.
(20) Moses, E.; Kume, T.; Hashimoto, T. *Phys. Rev. Lett.* **1994**, *72*, 2037.
(21) Stein, R. S.; Rhodes, M. B. *J. Appl. Phys.* **1960**, *31*, 1873.
(22) Stein, R. S.; Wilson, P. R. *J. Appl. Phys.* **1962**, *33*, 1914.
(23) Hashimoto, T.; Fujioka, K. *J. Phys. Soc. Jpn.* **1991**, *60*, 356.
(24) Saito, S.; Hashimoto, T.; Morfin, I.; Lindner, P.; Boue, F. *Macromolecules* **2002**, *35*, 445.
(25) Hashimoto, T.; Kume, T. *J. Phys. Soc. Jpn.* **1992**, *61*, 1839.
(26) Kume, T.; Hashimoto, T. In *Flow-Induced Structure in Polymers*; Nakatani, A. I., Dadmun, M. D., Eds.; American Chemical Society: Washington, DC, 1995; p 35.
(27) Kume, T.; Hashimoto, T.; Takahashi, T.; Fuller, G. G. *Macromolecules* **1997**, *30*, 7232.
(28) Yanase, H.; Moldenaers, P.; Mewis, J.; Abetz, V.; van Egmond, J.; Fuller, G. G. *Rheol. Acta* **1991**, *30*, 89.

MA050092I